Cell Calcium 117 (2024) 102831

Contents lists available at ScienceDirect

Cell Calcium

journal homepage: www.elsevier.com/locate/ceca

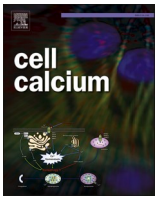

Allosteric changes in protein stability and dynamics as pathogenic mechanism for calmodulin variants not affecting Ca^{2+} coordinating residues

Christina Vallentin Holler [a,1,2], Nina Møller Petersson [a,1,3], Malene Brohus [a], Miska Aleksanteri Niemelä [b], Emil Drivsholm Iversen [a], Michael Toft Overgaard [a], Hideo Iwaï [b,4], Reinhard Wimmer [a,*]

[a] Department of Chemistry and Bioscience, Aalborg University, Frederik Bajers vej 7H, 9220 Aalborg, Denmark
[b] Institute of Biotechnology, University of Helsinki, PO Box 65, Helsinki, FIN-00014, Finland

ARTICLE INFO

Keywords:
Calmodulin
Cardiac arrhythmia
Calcium-sensing
Calmodulinopathy
Folbigg case

ABSTRACT

Mutations in the small, calcium-sensing, protein calmodulin cause cardiac arrhythmia and can ultimately prove lethal. Here, we report the impact of the G113R variant on the structure and dynamics of the calmodulin molecule, both in the presence and in the absence of calcium. We show that the mutation introduces minor changes into the structure of calmodulin and that it changes the thermostability and thus the degree of foldedness at human body temperature. The mutation also severely impacts the intramolecular mobility of calmodulin, especially in the apo form. Glycine 113 acts as an alpha-helical C-capping residue in both apo/ - and Ca^{2+}/ calmodulin, but its exchange to arginine has very different effects on the apo and Ca^{2+} forms. The majority of arrhythmogenic calmodulin variants identified affects residues in the Ca^{2+} coordinating loops of the two C-domain EF-Hands, causing a 'direct impact on Ca^{2+} binding'. However, G113R lies outside a Ca^{2+} coordinating loop and acts differently and more similar to the previously characterized arrhythmogenic N53I. Therefore, we suggest that altered apo/CaM dynamics may be a novel general disease mechanism, defining low-calcium target affinity – or Ca^{2+} binding kinetics – critical for timely coordination of essential ion-channels in the excitation-contraction cycle.

Significance Statement

Calmodulin regulates numerous calcium-dependent processes, with the human heartbeat being a prominent example. Mutations in calmodulin are linked with cardiac arrhythmia. One such mutation, G113R, is uncharacteristically located away from the Ca^{2+} coordinating loop.

We report new insights into the effect of the mutation on the structure and dynamics of calmodulin in its calcium-free and calcium-bound forms, offering molecular-level explanations for the changes in behavior of this variant. The results point at a new mechanism for how mutations in calmodulin can exert a deleterious influence on the cardiac cycle. The dynamics of the calmodulin molecule is of critical importance. Thus, the exact degree of structural flexibility cannot be altered in either direction without potentially life-threatening disturbances of its function.

* Corresponding author: Aalborg University, Frederik Bajers vej 7H, 9220 Aalborg, Denmark.
E-mail address: rw@bio.aau.dk (R. Wimmer).
[1] These authors contributed equally.
[2] Current address: Biogenity, Niels Jernes vej 10, 9220 Aalborg, Denmark.
[3] Current address: Agilent Technologies, Produktionsvej 42, 2600 Glostrup, Denmark.
[4] Current address: Orion Corporation Orion Pharma, Orionintie 1, PO Box 65, FI-02200, Espoo, Finland.

https://doi.org/10.1016/j.ceca.2023.102831
Received 11 September 2023; Received in revised form 10 November 2023; Accepted 12 November 2023
Available online 14 November 2023

1. Introduction

Calmodulin (CaM) is a calcium binding protein that plays a key role as universal Ca^{2+} sensor and mediator of signaling in all living organisms. Its 148 amino acids are distributed in two lobes acting largely independent of each other. The N-lobe has a lower affinity for Ca^{2+} than the C-lobe, empowering CaM to sense calcium concentrations ($[Ca^{2+}]$) over a wide range. Moreover, the kinetics of Ca^{2+} dissociation are widely differing: while the N-lobe displays fast Ca^{2+} dissociation at $\approx$1000 s^{-1}, C-lobe Ca^{2+} dissociation occurs much slower at $\approx$11.8 s^{-1}. This ability to bind calcium with high specificity over a wide range of $[Ca^{2+}]$ and time scales coupled to its profound structural changes upon Ca^{2+} binding makes it the most widely utilized Ca^{2+} signaling protein with >350 known targets [1,2]. The role as a ubiquitous intracellular Ca^{2+} sensor might be what drives the extraordinary conservation of CaM. In fact, all vertebrates possess CaM with an identical amino acid sequence, emphasizing the strong evolutionary pressure against any changes in CaM. Moreover, humans have three genes (*CALM1–3*) encoding for exactly the same CaM protein product. Nevertheless, in 2012, the first human CaM missense variants were discovered in individuals suffering from cardiac arrhythmia and sudden death [3].

CaM plays a key role in the generation of the heartbeat, where its Ca^{2+}-dependent interaction with several ion channels makes up an immensely finely tuned control mechanism. Here, calmodulin Ca^{2+}-sensing ensures opening and closing of the individual channels at exactly the needed points in time during the cardiac cycle. The role of CaM in the heartbeat has been reviewed in depth [4] and shall not be described here. Suffice it to say that the voltage gated sodium channel, $Na_V1.5$, the voltage gated potassium channel $K_V7.1$, the voltage gated calcium channel $Ca_V1.2$ and the ryanodine receptor (the sarcoplasmic reticulum calcium release channel, despite its name) RyR2 are among the key cardiac ion channels, and they all depend on CaM-mediated Ca^{2+} signaling for their correct working. Any disturbance in this finely tuned system will lead to malfunctioning that is experienced as cardiac arrhythmia or even cardiac arrest. Under a regime of constantly changing $[Ca^{2+}]$, this goes for disturbances in affinities as well as disturbances in kinetics, both of which can lead to delayed (or premature) signaling. Owing to the explosive developments in genome sequencing, a number of CaM mutations has been identified, some of them carried by patients with cardiac diseases, others identified in patients with neurological diseases, and yet others in larger sequence repositories without any phenotype description or recognized disease symptoms [5,6]. Mechanistically, all hitherto investigated CaM mutations leading to cardiac phenotypes dysregulate the opening and closing of either $Ca_V1.2$ or RyR2 or both [7–9].

A CaM variant, that recently has reached some notoriety, is CaM-G113R,[5] since it has come to play a central role in an Australian legal case about infanticide [10,11]. Briefly, an Australian woman was tried and convicted of murdering her four infants, despite of her maintaining her innocence. Later, it turned out that two of the children inherited a *CALM2* G113R variant from the mother. Investigation of the impact on protein function suggested that the G113R variant would likely be arrhythmogenic, and may have caused cardiac arrest in the two children [11]. Publication of these data resulted in a decision to open a hearing into the conviction, which took place in late 2022 and early 2023 where scientists were called to give evidence (https://2022folbigginquiry.dcj.nsw.gov.au/exhibits.html). Following the conclusion of the hearing, in June 2023, the woman was pardoned and released from prison [12].

Extensive biophysical investigations [11] proved that the function of the G113R variant of CaM is indeed altered in that its Ca^{2+} binding affinity is reduced, its affinity for the CaMBD2 binding site of RyR2 is lower over the whole range of physiologically relevant $[Ca^{2+}]$, but the effect is most pronounced at low and intermediate $[Ca^{2+}]$ and also its affinity for the IQ motif of $Ca_V1.2$ is lower at low and intermediate $[Ca^{2+}]$. The ability of CaM to close $Ca_V1.2$ and RyR2 is severely affected by the mutation. Further, the affinity for the IQ-domain of $Na_V1.5$ is reduced, primarily at low $[Ca^{2+}]$ [13].

The G113 residue is located in a loop, it is not directly involved in Ca^{2+} binding, it is not even in the vicinity of a Ca^{2+}-binding site. The molecular mechanism by which the mutation disturbs protein function, is thus not obvious. In addition, the mutation occurs in a different part of the molecule than the arrhythmogenic mutations investigated so far. Therefore, we set out to investigate the influence of the G113R mutation on the structure and molecular dynamics of the CaM protein.

Previous investigations of CaM variants demonstrated clearly that mutations only affect the lobe, they are located in, while the structure and dynamic of the other lobe is unchanged [14,15]. Therefore, and to simplify and accelerate data analysis, we developed a new approach to investigate a segmentally isotopically labeled version of CaM, where only amino acids Ser81-Lys148 are isotopically labeled, while amino acids 1–80 are present, but without isotope labeling. This was achieved by protein *trans*-splicing.

2. Results

2.1. Segmental labeling of calmodulin

The production of segmentally isotope-labeled CaM by incorporating ^{13}C,^{15}N only into the C-lobe of the CaM and its variant was successful. Figure S1 demonstrates the comparison of the ^{15}N-HSQC spectra between the fully and segmentally labeled Ca/CaM-wt, manifesting that the chemical shifts of the C-lobe are identical, indicative of an identical, undisturbed, structure of CaM even if produced segmentally. The simplification of NMR spectra becomes evident immediately. Fig. 1 shows the changes introduced into the ^{15}N-HSQC spectra by the G113R mutation. It is clear that the mutation did not disrupt the fold of a large portion of calmodulin completely. This is also the conclusion based on CD spectra presented below.

Backbone and side-chain resonances were assigned for both apo/ and Ca/CaM-G113. Assignments were deposited in the BioMagResBank with accession numbers 34765 (apo/CaM-G113R) and 34764 (Ca/CaM-G113R).

2.2. G113R stabilizes apo/CaM

Chemical shift differences in the C-lobe of the G113R variant were calculated against the C-lobe of the N53I variant, because the C-lobe of N53I has an identical sequence and structure to the wild-type and its assignment was performed under very similar sample conditions to that of G113R [15] while there is no published assignment of apo/CaM wild-type. The data are shown in Figure S2A. The changes in chemical shift occur mainly in the immediate vicinity of the mutation site, from residues T110-L116, with a few amino acids further away affected, too (residues G98–Y99).

The structure of apo/CaM-G113R was solved by solution NMR. The coordinates were deposited into the PDB database with accession code 8BFG. Fig. 2A shows the structure of the C-lobe of apo/CaM-G113R compared to the C-lobe of apo/CaM-wt [16]. The overall structure is very similar. All secondary structure elements are intact, however, there are some subtle differences. Helices VII and VIII are on average 3.6 Å further apart from each other in the variant. Arginine 113 is oriented towards the ends of helices V and VIII, which is not the case for G113. We will explore the local changes around the mutation site in more detail in the Discussion section and compare them to changes occurring in Ca/CaM. CD spectra of apo/CaM wt and G113R shown in Fig. 2D

[5] There are different practices in literature on the numbering of CaM. Throughout this article, numbering follows the mature protein product, i.e. without counting the initial methionine residue. In the literature, the initial methionine is sometimes counted as amino acid number 1 and thus the same protein variant is also sometimes referred to as G114R.

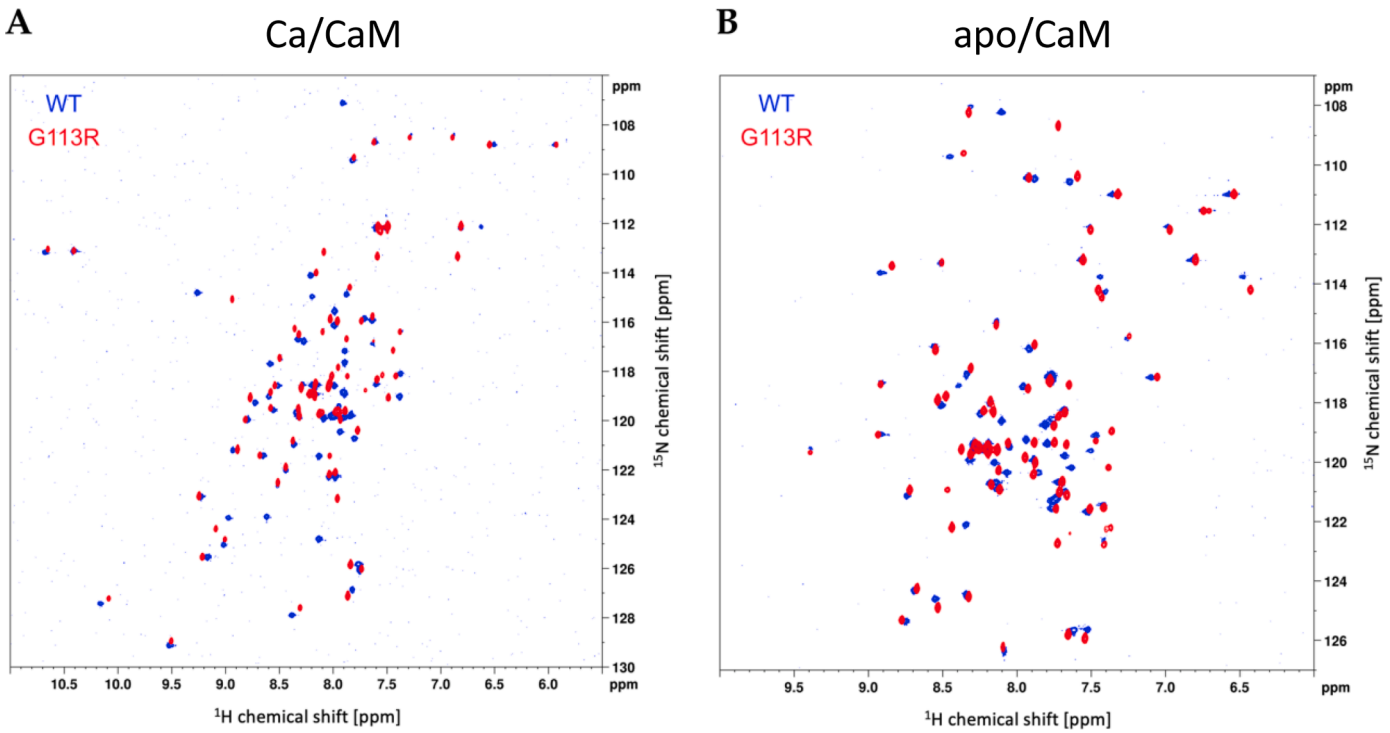

Fig. 1. Overlay of [^{1}H-^{15}N]-HSQC spectra of segmentally labelled (C-lobe U-^{15}N, ^{13}C) CaM-G113R (red) and (C-lobe U-^{15}N,20 % ^{13}C) CaM-WT (blue). A) Ca/CaM; B) apo/CaM.

corroborate the overall similarity of the structures, and even show a slight increase in secondary structure content from 58.3 % to 66 % as a consequence of the mutation.

Nuclear magnetic relaxation data shows a marked reduction in intradomain flexibility both on the ps-ns and the μs-ms time scales. The heteronuclear steady-state {^{1}H}−^{15}N-NOE data shown in Fig. 3A demonstrate a significant reduction in structural flexibility on the ps-ns time scale as almost all NOE values are higher for G113R than for the wild-type protein. Structural flexibility also decreases on the μs-ms timescale: while wild-type apo/CaM has numerous amino acids with sizeable exchange contribution to T_2 relaxation across its entire C-lobe, the apo/CaM-G113R variant exhibits only three amino acids with measurable exchange contributions, namely I100, T110 and Q143 (Fig. 3B). Together, these data suggest a dramatically decreased conformational flexibility of the C-lobe of apo/CaM-G113R throughout a wide range of timescales. The increased compactness of the variant is further underlined by ^{15}N-T_1 and T_2 data (Figures S3A and S4A, values have been deposited to the BioMagResBank). T_1/T_2 (Figure S5A) data allow for the calculation of the correlation time of overall molecular tumbling, τ_c [17]. The G113R variant shows more uniform values of T_1/T_2 along the sequence, which is consistent with a loss of slow conformational exchange. Based on these data, τ_c = 7.9 ns for apo/CaM-G113R, compared to τ_c = 8.7 ns for apo/CaM-wt, indicating a smaller hydrodynamic radius for the variant CaM.

Apo/CaM-G113R shows increased thermostability (Fig. 3C): the midpoint temperature of denaturation of the C-lobe goes from 45.5 ± 0.15 °C to 48.1 ± 0.3 °C ($p = 3.5 \times 10^{-6}$). with a concomitant increase of the enthalpy of unfolding, ΔH from 133.4 ± 1.9 kJ/mol to 159.5 ± 5.9 kJ/mol (p = 0.0002). The midpoint temperature of denaturation of the N-lobe does not change significantly (wt: 57.9 ± 0.2 °C, G113R: 58.1 ± 0.1 °C, p = 0.12), nor does the enthalpy of unfolding (wt: 204.1 ± 3.1 kJ/mol, G113R: 190.0 ± 8.8 kJ/mol (p = 0.02)). Figure S6 shows a statistical treatment of the data from individual runs.

2.3. G113R destabilizes Ca/CaM

Changes between the C-lobes of wild-type Ca/CaM and Ca/CaM-G113R occur mainly between amino acids R106-L116 (Figure S2B). The backbone H or N resonances of the variant could not be detected for a number of amino acids in this range: R106, H107, L112, R113 (and M124 outside this range). Other, weaker, changes in chemical shifts were observed for amino acids S81, E84, F92, A147 and K148.

The structure of Ca/CaM-G113R was solved by solution NMR. The overall structure is unchanged, however, there are some differences to the wild-type structure [18] (Fig. 4A). First, the loop between helices VI and VII, which carries the mutation site, is much more disordered in the variant CaM. This lack of order can already be seen at amino acid R106 which is located well into helix VI, and it increases from amino acid R106 towards the end of helix VI. Also, the N-terminal part of helix VII is slightly affected. More to the unexpected, the very C-terminus of CaM, helix VIII, also displays a diminished degree of order and a slightly tilted orientation. The sidechain of R113 does not have any defined orientation. The coordinates were deposited into the PDB database with accession code 8BD2.

Since the structure of Ca/CaM-G113R displayed a greater degree of disorder, we went on to record relaxation experiments in order to get more information about intramolecular flexibility. While wild-type Ca/CaM has no amino acids with sizeable exchange contribution to T_2 relaxation in its entire C-lobe, the Ca/CaM-G113R variant exhibits several amino acids with exchange contributions, located at the start of the C-lobe (S81-I85), around the mutation site and at the very C-terminus (Fig. 5A). This clear increase in intramolecular flexibility on the μs-ms timescale is, however, not accompanied by changes in intramolecular flexibility on the ps-ns timescale, as witnessed by heteronuclear NOE data (Fig. 5B). There is no overall trend in the NOE data, most amino acids show similar values within the error limits. For some amino acids, V108, T110 and E114, the NOE seems lower in the variant, for others, K115 and L116, the NOE of the G113R variant is higher. Due to rather weak signals in this part of the protein, the data carry a large uncertainty. The overall molecular tumbling of Ca/CaM-G113R is

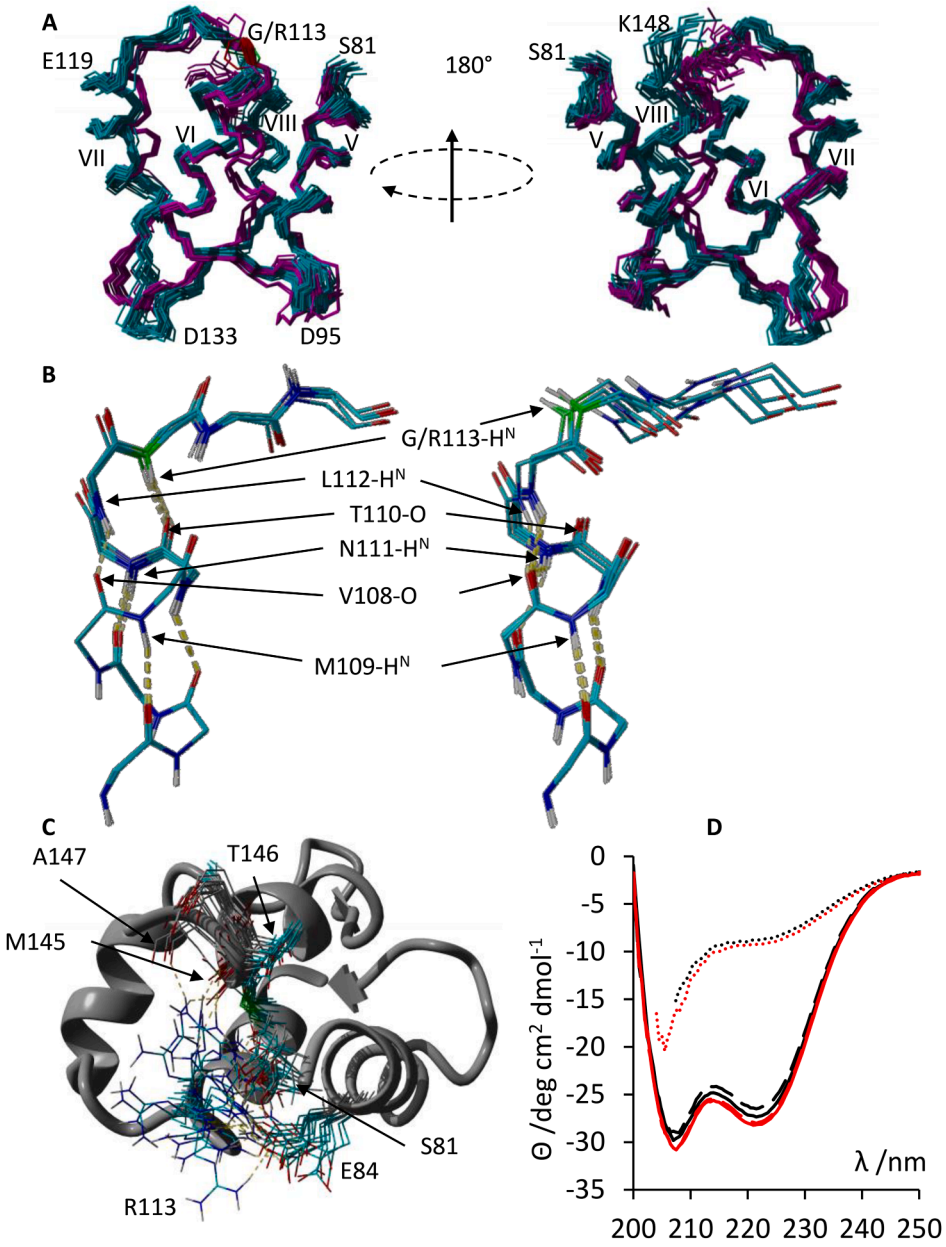

Fig. 2. A) Structure of the C-lobe of apo/CaM G113R (cyan) compared to apo/CaM wild-type (magenta, PDB ID 1CFC). The mutation site (aa 113) is shown in green (G113R) and red (wt). Helices are numbered with roman numerals. The bundles of 20 structures are overlaid and shown in two orientations. B) H-bond network in amino acids 105–115 of apo/CaM. wt is shown to the left, G113R to the right. The backbone nitrogen atom of amino acid 113 is shown in green. For better visibility, only the first five structures of the bundles are shown. C) apo/CaM G113R structure. One structure shown as cartoon, amino acids S81, E84, R113, M145, T146 and A147 shown for all 20 structures of the bundle. Hydrogen bonds are formed by R113-H^{η} to S81 O^{γ}, E84 O^{ε}, M145 O, T146 O and A147 O. D) Circular Dichroism spectra of apo/CaM wt (black) and G113R (red). Solid lines: CD at 25 °C before thermodenaturation, dotted lines: CD at 94 °C, dashed lines: CD at 25 °C after thermodenaturation.

slower (τ_c = 9.7 ns) than that of the wild-type (τ_c = 9.2 ns), as can be calculated from the T_1/T_2 ratio which is consistently higher in the variant (Figures S4B, S5B and S6B). This points at an increased hydrodynamic radius, consistent with increased intramolecular flexibility.

Due to the extraordinary stability of Ca/CaM, which remains partly folded at the boiling point of water, it is inherently challenging to study thermodenaturation of Ca/CaM in aqueous solution. We therefore recorded the thermodenaturation in the presence of 5 M urea, as has been done previously for studying other CaM mutations impact on Ca/CaM folding stability [19]. The CD spectra of Ca/CaM-wt and G113R at room temperature and 94 °C are shown in Fig. 5C. The ellipticity at 222 nm as a function of temperature is shown in Fig. 5D. In Ca/CaM, the C-lobe has higher thermostability, and is thus reflected in the second transition. T_m of the N-lobe changes from 52.9 ± 0.4 °C to 51.6 ± 0.1 °C (p = 0.007), while T_m of the C-lobe drops only slightly from 76.5 ± 0.4 °C to 74.1 ± 0.4 °C (p = 0.0002). Figure S7 shows the distribution of results. We cannot offer an explanation for the large change observed in the N-lobe in the presence of 5 M urea.

3. Discussion

How can we use the results presented here to understand the functional implications of the G113R mutation? To recapitulate, extensive biophysical investigation of CaM-G113R [11,13] has revealed that the mutation leads to 1) reduced affinity of CaM-G113 for Ca^{2+}, 2) reduced affinity of CaM-G113R for the $Ca_V1.2$ IQ domain at low and

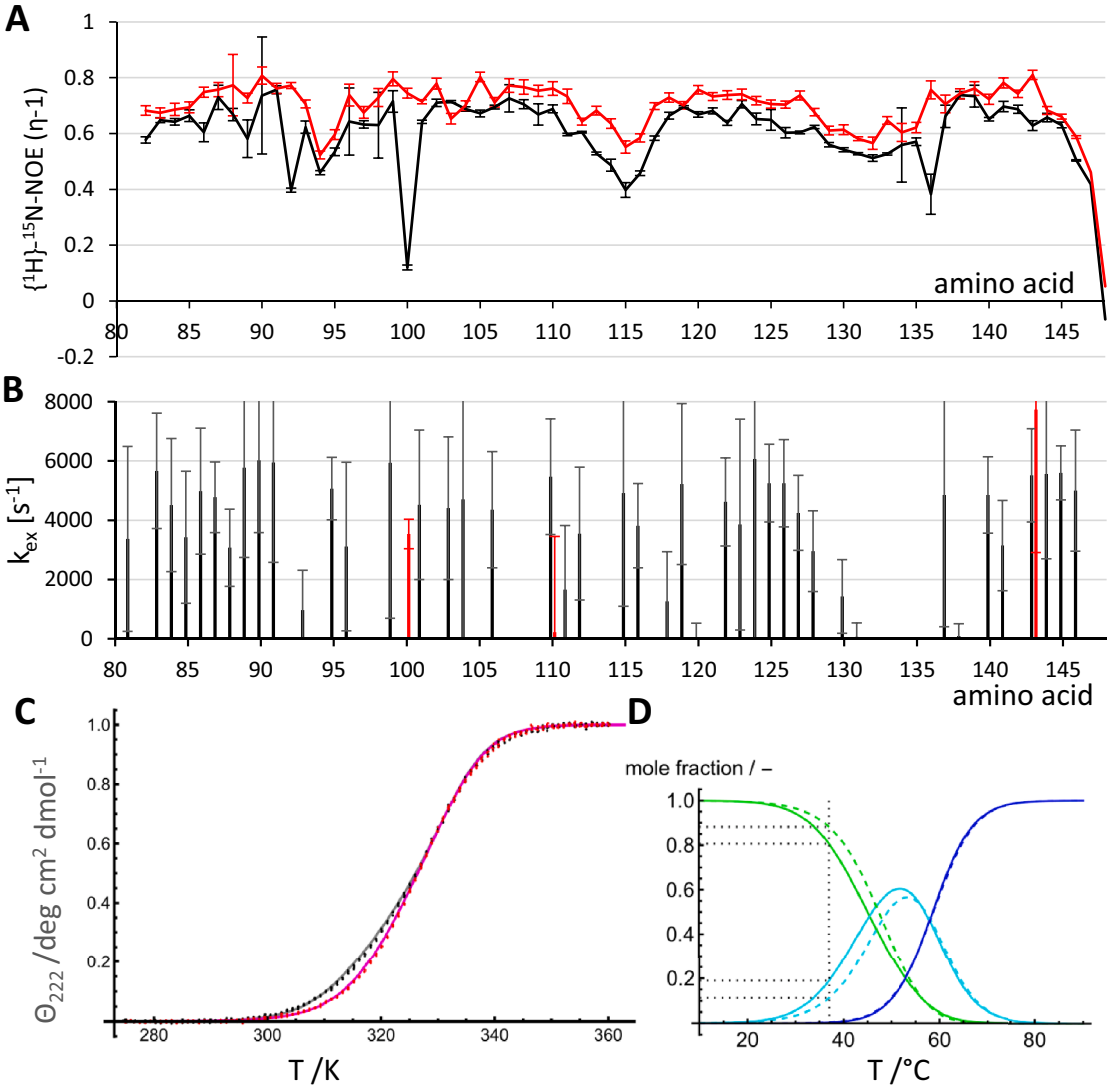

Fig. 3. A) Heteronuclear, steady-state $\{^1H\}-^{15}N$—NOE of apo/CaM-wt (black) and apo/CaMG113R (red). B) T_2-relaxation dispersion data of apo/CaM wt (black) and apo/CaM/G113R (red). C) apo/CaM mean residual ellipticity at 222 nm vs temperature. Data for the wild-type are shown in black, data for G113R in red. Individual datapoints from four independent experiments are shown as circles, the global fit is shown as line D) fraction of folded (green), partially unfolded (cyan) and denatured (blue) apo/CaM as a function of the temperature, based upon the results of the thermodenaturation experiment. Wild-type data are shown as solid lines, G113R as dashed lines. A vertical, black, dotted line indicates $T = 37$ °C.

intermediate, but not at high [Ca^{2+}], reduced affinity of CaM-G113R for the RyR2 CaMBD2 domain at low and intermediate [Ca^{2+}], 4) reduced affinity of CaM G113R for the $Na_V1.5$ IQ-domain, and 5) delayed closure of the cardiac calcium channels $Ca_V1.2$ and RyR2. Given that G113 is not directly involved in Ca^{2+} binding, it is rather enigmatic, how the G113R mutation can have such a profound effect on the functional properties of CaM.

3.1. G113 acts as a C-capping amino acid

G113 is located at the C-terminal end of α-helix VI both in apo/CaM and in Ca/CaM. In both structures, helix VI ranges from aa S101-N111. α-helices are stabilized by a number of hydrogen bonds from H^N of amino acid *i* to O of amino acid *i-4*. At the end of the helix, however, the chain turns away and proper hydrogen bonds cannot be formed. Various C-capping motifs exist at the end of an α-helix, and often, the capping amino acid adopts an α_L conformation ($\varphi > 0°$ and $\psi > 0°$)[20]. The α_L conformation of the capping amino acids serves a dual purpose: it allows for a last hydrogen bond from its H^N back to a helix backbone oxygen atom and it provides a new direction for the chain. Glycin is ideally suited at this position for two reasons: first, it experiences no conformational strain adopting the α_L conformation, and second, it allows for backbone solvation, i.e. the formation of H-bonds from backbone oxygen atoms to the solvent, in part making up for the missing intra-helix H-bonds[21]. Larger amino acids, in particular bulky hydrophobic amino acids, result in a conformational strain and unfavorable backbone solvation and are thus not well suited. Consequently, ≈1/3 of α-helices are capped by glycine[22,23]. His, Asn, Arg and Lys are not as unfavorable as hydrophobic amino acids, but far less favorable than Gly [21]. In both apo/CaM and Ca/CaM, G113 serves as a C-capping amino acid for helix VI. We therefore hypothesize that replacing the C-capping glycine by an arginine should manifest itself in an effect on the stability of the helix and on the local geometry of the protein backbone.

3.2. Replacing glycine 113 by arginine has opposite effects on apo/ and Ca/CaM, respectively

A first line of evidence for G113R imposed changes can be seen from looking into the H-bonds of Helix VI (Figs. 2B and 4B): L112-H^N forms a H-bond with M109-O both in the wild-type and the G113R variant. Such

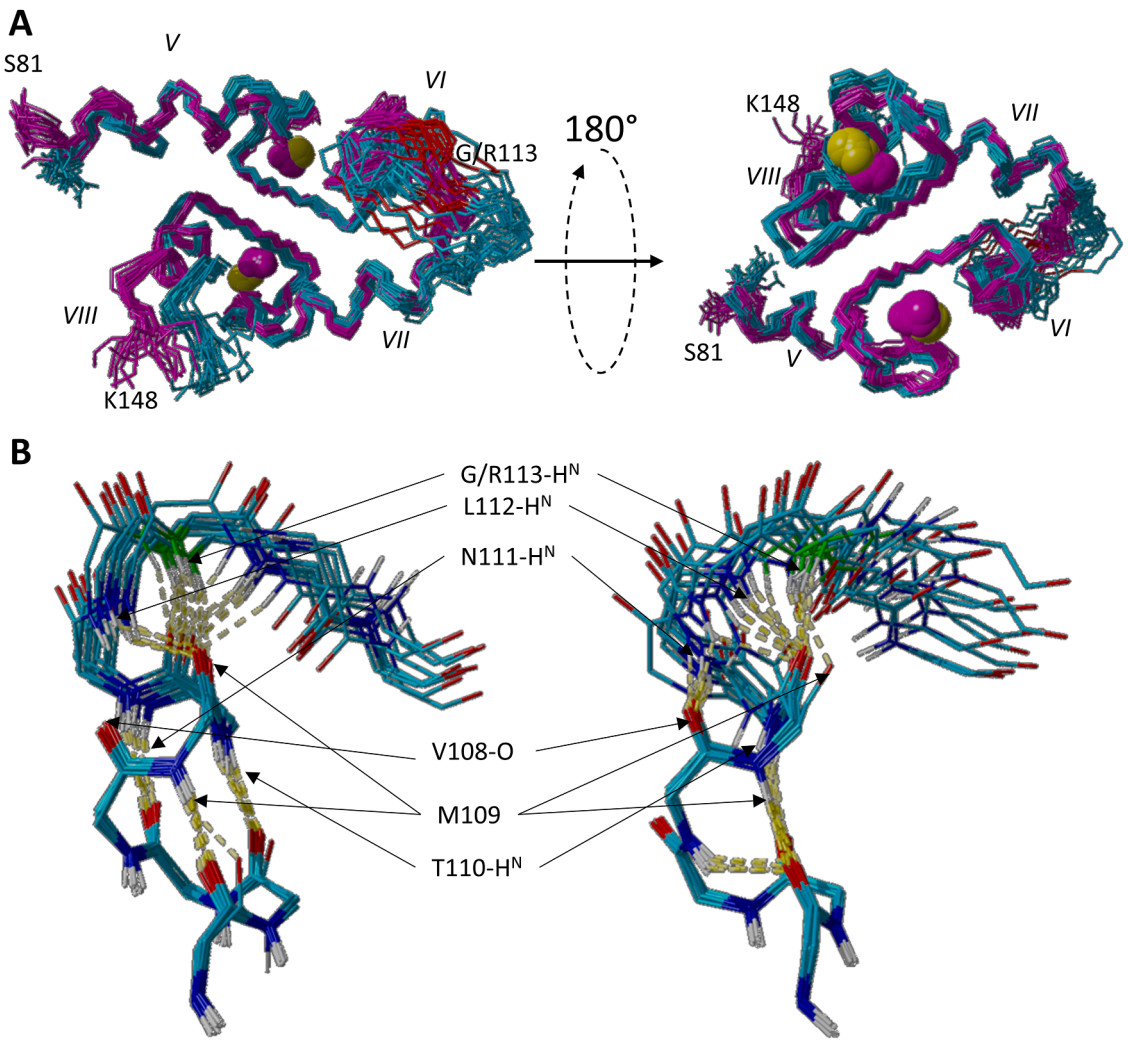

Fig. 4. A) Structure of the C-lobe of Ca/CaM G113R (cyan) compared to wild-type (magenta, PDB ID 1X02). The mutation site (aa 113) is shown in green (G113R) and red (wt). Helices are numbered with roman numerals. The bundles of 20 structures are overlaid and shown in two orientations. B) H-bond network in amino acids 105–115 of Ca/CaM. wt is shown to the left, G113R to the right. The backbone nitrogen atom of amino acid 113 is shown in green. For better visibility, only the first five structures of the bundles are shown.

a hydrogen bond from H^N of amino acid *i* to O of amino acid *i-3* is consistent with a 3_{10}-helical conformation, often found at the end of α-helices. In Ca/CaM wt, N111-H^N is H-bonded to H107-O in 18/20 structures, but V108-O in the remaining two structures of the bundle. In Ca/CaM G113R, N111-H^N is H-bonded to V108-O in all structures of the bundle, thus it seems that the onset of a 3_{10}-helical conformation is shifted by one amino acid. For the following amino acids, the H-bonding pattern diverges: while wt-CaM features H-bonds from G113-H^N to T110-O in 19 out of 20 structures in the bundle, and also from E114-H^N to 110-O (7/20 structures), the altered geometry around amino acid 113 in the G113R variant leads to H-bonds from R113-H^N to M109-O (15/20 structures), but no H-bonds are found involving E114-H^N. The missing backbone amide resonances in amino acids preceding R113 further underlines the lack of structural stability introduced locally due to the mutation.

Further, the G113R mutation leads to clear changes in the local backbone conformation. Figure S7 illustrates the backbone φ/ψ angle distribution of amino acids M109-K115. Outside this range, the backbone φ/ψ angles do not differ significantly between wild-type and G113R variant, neither in apo/CaM nor in Ca/CaM. The increased backbone flexibility indicated by relaxation data is also reflected in the φ/ψ angle distribution across the 20 structures in the bundle. M109 and L112 display conformations over a wide range of ψ angles, while T110 and N111 remain in helical conformation. The φ/ψ angles of amino acid 113 change for Ca/CaM: in the wild-type, G113 adopts a classical α_L conformation. In the variant, however, R113 has moved to a different, more favorable region of the Ramachandran plot, adopting an extended, β-strand like, conformation, similar to E114 which features this conformation in both wt and G113R. Possibly to facilitate the turn towards the next helix, or possibly to minimize electrostatic repulsion with R113, K115 adopts a range of conformations across the bundle, including an α_L conformation in some conformers, while it continues the elongated β-strand conformation in the wild-type.

Intriguingly, the G113R substitution does not have the same effect on local geometry in apo/CaM, even though G113 also is located at the end of an α-helix in apo/CaM. The H-bond pattern in apo/CaM wt (Fig. 2B) is similar to Ca/CaM wt in this region: H^N of G113 forms a H-bond with T110-O, and H^N of L112 forms a H-bond with V108-O only in 2 out of 20 structures. N111-H^N forms a H-bond with H107-O. Neither E114-H^N nor M109 O take part in a hydrogen bond. The only change in H-bonding pattern is that R113-H^N does not form any medium-range H-bonds, while L112-H^N and V108-O form H-bonds in all 20 variant structures. H-bonds from N111 do not change due to the mutation. Looking at φ/ψ angles (Figure S7), it becomes evident that the major change in backbone conformation in apo/CaM is happening for L112, which goes from a helical to an extended, β-strand like, conformation, while R113

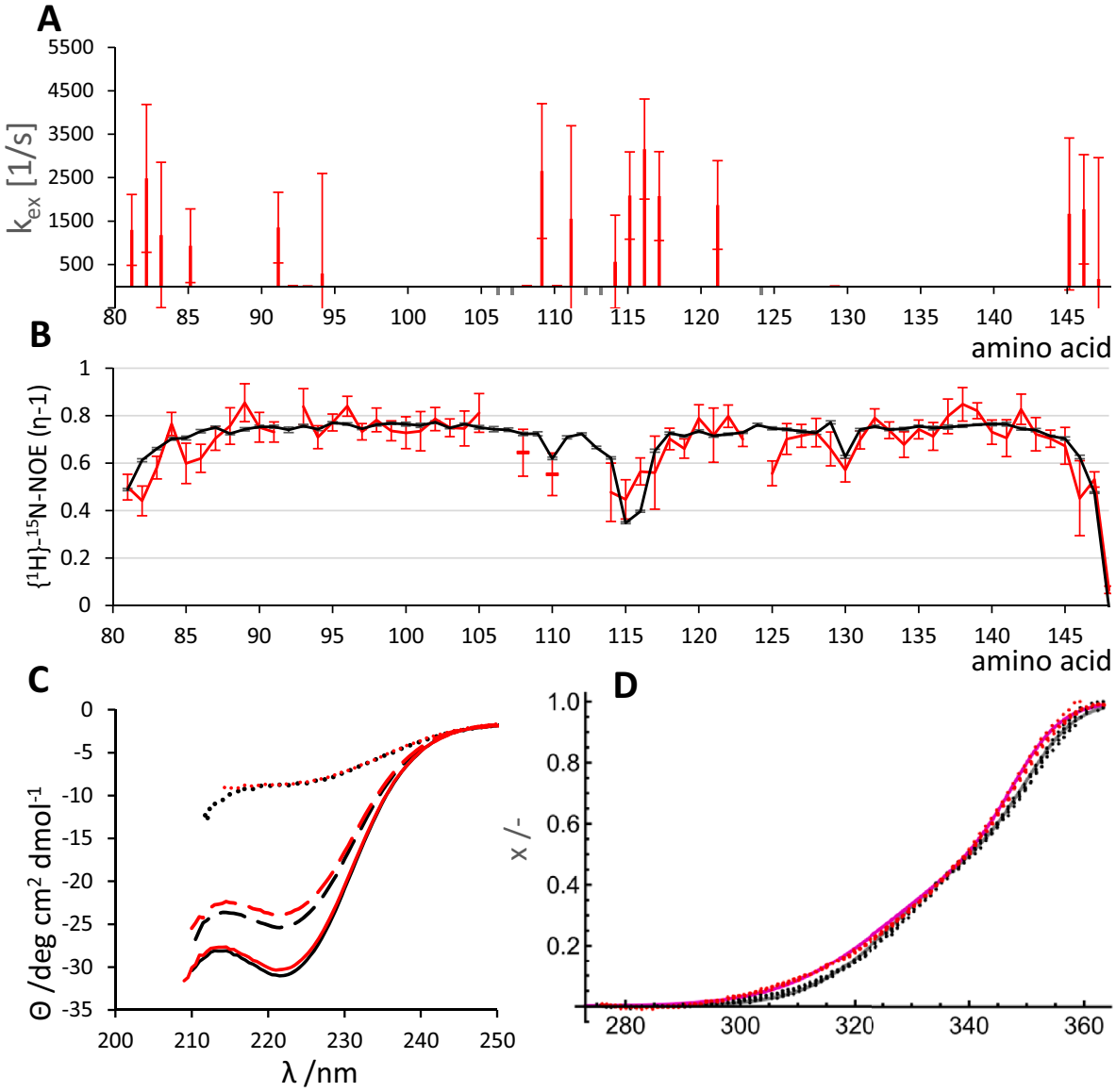

Fig. 5. Structural flexibility of the C-lobe of Ca/CaM-G113R compared to the wild-type A) Heteronuclear, steady-state {^{1}H}−^{15}N—NOE of Ca/CaM-wt (black) and Ca/CaM-G113R (red). B) T_2-relaxation dispersion data of Ca/CaM wt (black) and Ca/CaM-G113R (red). Amino acids, for which no value could be determined, are shown with a gray bar at −200 just to distinguish them from amino acids without an exchange contribution to T_2 C) Circular Dichroism spectra of Ca/CaM wt (black) and G113R (red) in the presence of 5 mM CaCl2 and 5 M urea. Solid lines: CD at 25 °C before thermodenaturation, dotted lines: CD at 94 °C, dashed lines: CD at 25 °C after thermodenaturation D) Ca/CaM mean residual ellipticity at 222 nm from all four experiments, normalized to the degree of folding vs temperature. Data for the wild-type are shown in black, data for G113R in red. The fitted curves are shown in gray for wild-type and in magenta for G113R.

remains in α_L conformation, different from what is happening in Ca/CaM G113R. E114, whose conformation is not very well defined in the wild-type structure, adopts a combination of φ/ψ angles that is not in the favored regions of the Ramachandran plot, similar to that of K115 in the wild-type structure. However, in apo/CaM G113R, K115 adopts a helix-like conformation. Consequently, helix VII is not disturbed and starts at T117 both in the wild-type and in G113R. The obvious question is, what might cause this difference: the answer can be found in the possible interactions that the guanidine-group of R113 can form with other parts of CaM! Fig. 2C shows the orientation of side chain R113 in all 20 structures. R113 forms hydrogen bonds and salt bridges to: E84 O^{ε} (16/20 structures), S81 O^{γ} (5/20 structures), M145 O (3/20), T146 O (1/20) and A147 O (1/20 structures). In some structures, R113 forms H-bonds not only with H^{η}, but in addition with H^{ε} as donor. This ability to form a number of interactions likely explains the reduced conformational flexibility of the G113R variant in the apo form. In Ca/CaM G113R, only H-bonds of R113-H^{η} to E120 O^{ε} (8/20 structures) and E123 O^{ε} (3/20 structures) can be observed, and they seem rather to distort helix VII than contribute to stability. E84 is located too far away in Ca/CaM to interact with R113. The electrostatic interaction of the patch of three glutamates E82-E84 was identified as important for the regulatory activity of CaM [24], and it can be speculated that the interaction with R113 could disturb this interaction and thus the regulatory pathways.

3.3. *Changes in CaM explain changes in Ca^{2+} affinity*

We have now seen that the C-lobe of apo/CaM G113R shows increased thermostability, while the C-lobe of Ca/CaM G113R shows a reduced thermostability (in the presence of 5 M urea). This means that the ΔG of Ca^{2+} binding, the difference between ΔG of the apo form and ΔG of the Ca form decreases, which ultimately manifests itself in a higher K_d value for Ca^{2+}-binding. (Fig. 6). This can explain the reduced

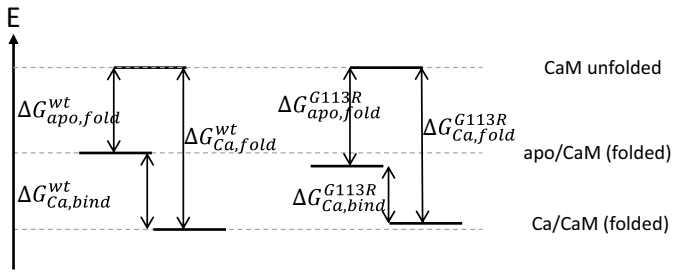

Fig. 6. Energy-level diagram of CaM in the folded and unfolded states for the wild-type (left) and variant (right), illustrating the impact of changes in molecular stability on calcium binding. $\Delta G_{apo,fold}$: ΔG of folding for apo/CaM, $\Delta G_{Ca,fold}$: ΔG of folding for Ca/CaM, $\Delta G_{Ca,bind}$: ΔG of Ca-binding of CaM.

affinity of CaM G113R for Ca^{2+} even though G113R does not directly take part in Ca^{2+} binding.

3.4. Changes in backbone flexibility could be responsible for altered CaM interactions

Structural flexibility of proteins is often a contributing factor to substrate binding, because it allows the protein molecule to sample a range of conformations, some of which can be close to the substrate-bound conformation and thus predestined for substrate binding. It can be speculated that the reduced flexibility of apo/CaM-G113R could lead to a lower population of such states primed for substrate interaction and thus weaken or delay such interactions. Many proteins with important function occur as intrinsically disordered protein, their disorder being vital for their ability to correctly interact with target molecules [25–27]. CaM is not usually seen as intrinsically disordered protein, however, the midpoint of denaturation, T_m, of apo/CaM-wt C-lobe is so low, that a sizeable fraction of the protein molecules is disordered at human body temperature. Fig. 3D shows the distribution of folded, partially unfolded (C-lobe unfolded, N-lobe folded) and completely denatured apo/CaM as a function of temperature. At 37 °C, 80.6 % of the CaM-wt molecules in an ensemble are folded, whereas 19.1 % are partially unfolded, with their N-lobe folded and their C-lobe unfolded. For the G113R variant, 88.2 % of molecules are folded, and only 11.4 % are partially unfolded. If disorder is vital to ensure substrate binding, this lower population of the partially disordered state can lead to slower k_{on} and thus higher K_d values for the interaction of apo/CaM-G113R with various intracellular targets. In fact, we have previously studied CaM variants with altered intramolecular mobility (Fig. 7) demonstrating that the F141L variant behaves in a similar manner, just in the opposite direction: it disrupts the tertiary structure of the C-lobe of apo/CaM, effectively rendering it a molten globule[14]. This ultimately leads to a greatly increased affinity of apo/CaM to $Ca_V1.2$, which is the underlying reason for the disturbance in the regulation of the cardiac cycle, leading to LQT-syndrome. Less dramatic, and in the other lobe, the N53I variant also shows altered backbone dynamics and a destabilized lobe, leading to changes in CaM interaction with RyR2, dysregulation of RyR2 Ca^{2+}-gating properties, and ultimately to CPVT[3,9,15,28]. The regulation of cardiac rhythm has evolved to take advantage of all aspects of the CaM molecule and even small changes in dynamics can interfere unfavorably with the delicate interplay of all the different interactions that the CaM molecule has to perform with immaculate timing in order to ensure a healthy cardiac rhythm.

4. Materials and methods

4.1. Calmodulin production and purification

The N-lobe (amino acids 1–80) and C-lobe (amino acid 81–148) were produced separately as intein-fusion proteins [29], each with its part of a split intein from T4-like bacteriophages of *Aeromonas salmonicida* [30]. After *trans*-splicing and purification, a native CaM molecule was obtained with residues 81–148 doubly [^{13}C,^{15}N]-labeled, while the residues 1–80 are unlabeled. The constructs and methods are described in detail in the Supplementary Material.

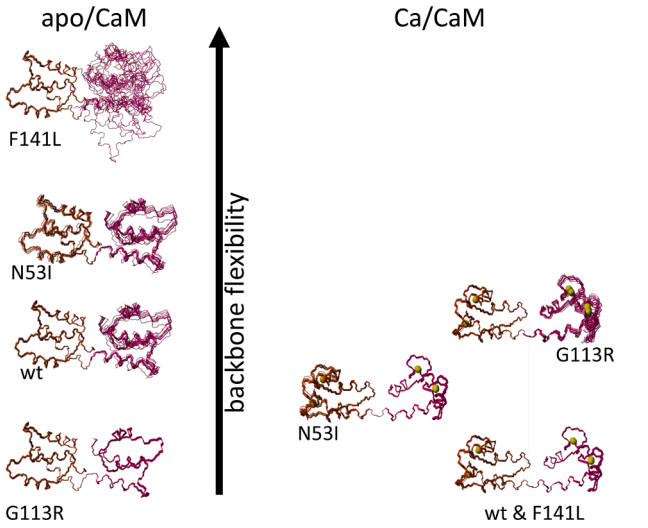

Fig. 7. Backbone flexibility of CaM variants in apo and Ca-forms. The N-lobe of CaM is shown in orange and the C-lobe in magenta. Flexibility is only indicated as general fuzziness and not displayed on a residue-specific level.

4.2. NMR sample preparation

Ca/CaM-G113R: The sample contained 1 mM Ca/CaM-G113R, 5 mM $CaCl_2$, 100 mM KCl, 2 mM NaN_3, 0.1 mM 2,2,3,3-tetradeutero-3-(trimethylsilyl) propionate (TSP-d_4) dissolved in 20 mM HEPES. The sample contained 5 % (v/v) D_2O, the pH was 6.69.

Apo/CaM-G113R: The sample contained 1.2 mM apo/CaM-G113R, 5 mM EDTA, 100 mM KCl, 5 mM NaN_3, 0.1 mM TSP-d_4 dissolved in 20 mM HEPES. The sample contained 5 % (v/v) D_2O, the pH was 6.64.

4.3. NMR

All NMR spectra were recorded on a BRUKER AVIII-600 MHz spectrometer equipped with a 5 mm TCI-CPP probe with z-gradient coil. All experiments were recorded at 298.1 K. Spectra were recorded and processed in Topspin 3.6.2 and 3.6.4. Relaxation data were processed and analyzed using BRUKER Dynamics Center 2.7.1. The following spectra were recorded for both samples: ^{15}N-HSQC, ^{13}C-HSQC (aliphatic and aromatic), HNCO, HN(CA)CO, CBCA(CO)NH, HNCA, CBCANH, 2D-CACO, HBAH(CBCACO)NH, (H)CC(CO)NH, H(CCCO)NH, (HB)CB (CGCD)HD, (HB)CB(CGCDCE)HE, 3D-^{15}N-HSQC—NOESY ($\tau_m = 75$ ms), 3D-^{13}C-HSQC—NOESY (aliphatic: $\tau_m = 100$ ms; aromatic: $\tau_m = 120$ ms), ^{15}N-T_1 with relaxation delays (100; 200; 300; 500; 800; 1300; 2300; 3500 ms), ^{15}N-T_2 relaxation delays (16.96; 33.92; 67.84; 135.68; 169.6; 203.52; 237.44; 271.36 ms), {^1H}–^{15}N-NOE [31] and ^{15}N-T_2-CPMG relaxation dispersion experiments [32] with a constant relaxation delay τ_{CPMG} of 40 ms (2 × 20 ms) and CPMG field strengths ranging from 0 to 1150 Hz (0; 150; 250; 350; 450; 600; 750; 900; 1000; 1150 Hz) with all field strengths except 0 Hz conducted twice in pseudo-randomized order. In addition, a tyrosine-selective (HB)CB(C^{aro})H^{aro} experiment was recorded for Ca/CaM-G113R.

4.4. Assignment and structure determination

Ca/CaM: sequential assignment was performed by the sequential walk method applied to triple resonance spectra using CARA 1.8.4.2

[33,34]. The NEASY module was used to collect and integrate NOESY cross-peaks.

Apo/CaM: automated sequential assignment was performed by the implementation of ARTINA on NMRtist [35] followed by manual curation using CARA. NOESY peaklists were picked by ARTINA and curated and integrated using the NEASY module of CARA.

For both conditions, FLYA and CYANA 3.97 [36–40] was used for simultaneous automated assignment of NOEs and structure calculation. TALOS-N [41] was utilized to derive backbone torsion angle restraints from chemical shifts. The resulting restraints were included in the structure calculation with FLYA and the subsequent refinement. Out of 100 calculated structures, the 20 structures with the lowest residual target function were used for refinement with YASARA 21.12.19 [42]. Refinement was performed in two steps: first *in vacuo* using the NOVA force-field [43] and then in explicit water using the YASARA force field [44].

4.5. Circular dichroism

Protein unfolding during thermodenaturation was measured by circular dichroism using a Chirascan Plus CD-spectrometer (Applied Photophysics), with a TC 125 temperature control unit (Quantum Northwest) and a AWC100 recirculating cooler (Julabo). Samples of 25 μM apo/CaM (wt and G113R) were prepared in a buffer containing 20 mM HEPES, 100 mM KCl and 0.5 mM EDTA at pH 7.2, while Ca/CaM (wt and G113R) samples were prepared in a buffer containing 20 mM HEPES, 100 mM KCl, 5 M urea and 1 mM $CaCl_2$ at pH 7.2.

CD spectra were measured in a range from 180 – 260 nm in duplicate prior to thermodenaturation at 25 °C and post thermodenaturation at 94 °C and again after cooling to 25 °C, with the following settings: 0.5 nm step size, 1 nm bandwidth and 0.25 s time-per-point. A temperature ramp was performed from 1 – 94 °C, with a rate of 0.5 °C/min, a 1 °C step, a 0.15 °C tolerance and an initial 300 s settling time. Ellipticity was measured at $\lambda = 222$ nm, 1 nm bandwidth and 1 s time-per-point. Ellipticity at $\lambda = 222$ nm was plotted against the temperature measured directly inside the solution. Thermodenaturation was performed four times for each variant under both apo and Ca^{2+} loaded conditions. The data were fitted to a three-state model using Wolfram Mathematica 13.1 based on the equations described by Greenfield [45]. Strictly speaking, the equations are only valid for a reversible unfolding process, and the data show that the process is close to 100 % reversible for apo/CaM, but only ~75 % for Ca/CaM. The fitting was performed in two steps: at first, both T_m, ΔH and Δc_p for both transitions were fitted for all four repetitions. In the second step, Δc_p was fixed to the average value of the four individual fits and only T_m and ΔH were fitted. For apo/CaM, the first transition belongs to the C-lobe and the second transition belongs to the N-lobe, which is more stable in the apo form. In Ca/CaM, the order of stability is reversed with the N-lobe denaturing before the C-lobe [46].

CRediT authorship contribution statement

Christina Vallentin Holler: Validation, Formal analysis, Investigation, Data curation, Writing – original draft, Writing – review & editing, Visualization, Funding acquisition. **Nina Møller Petersson:** Validation, Formal analysis, Investigation, Data curation, Writing – original draft, Writing – review & editing, Visualization, Funding acquisition. **Malene Brohus:** Conceptualization, Validation, Formal analysis, Investigation, Data curation, Writing – original draft, Writing – review & editing, Visualization, Supervision. **Miska Aleksanteri Niemelä:** Validation, Formal analysis, Investigation, Data curation, Writing – review & editing, Supervision. **Emil Drivsholm Iversen:** Validation, Formal analysis, Investigation, Data curation, Writing – original draft, Writing – review & editing, Visualization. **Michael Toft Overgaard:** Conceptualization, Methodology, Validation, Formal analysis, Investigation, Resources, Data curation, Writing – original draft, Writing – review & editing, Visualization, Supervision, Funding acquisition. **Hideo Iwaï:** Conceptualization, Methodology, Validation, Formal analysis, Investigation, Resources, Data curation, Writing – original draft, Writing – review & editing, Visualization, Supervision, Project administration, Funding acquisition. **Reinhard Wimmer:** Conceptualization, Methodology, Software, Validation, Formal analysis, Investigation, Resources, Data curation, Writing – original draft, Writing – review & editing, Visualization, Supervision, Project administration, Funding acquisition.

Declaration of Competing Interest

MTO acted as expert witness for the defense in the 2022/2023 Inquiry into the convictions of Kathlen Megan Folbigg (https://2022folbigginquiry.dcj.nsw.gov.au/). CVH, NMP and HI are employees of private companies.

Data availability

NMR assignments were deposited to the BioMagResBank with IDs 34765 (apo/CaM G113R) and 34764 (Ca/CaM G113R). Protein structures and NOE peak lists were deposited to the PDB with IDs 8BFG (apo/CaM G113R) and 8BD2 (Ca/CaM G113R).

Acknowledgments

We wish to thank Julia Johannson for her assistance in generating the plasmids used. This work was supported by the Novo Nordisk Foundation (RW: NNF18OC005303, MTO: NNF17OC0027550), the Academy of Finland (HI: 137995, 277335), the INSTRUCT-ERIC program for transnational access (RW/HI: PID 13849, VID 24616), the Danish Council of Independent Research | Natural Sciences (MTO: 2032-00333B), Lundbeck Foundation (MTO: R324-2019-1933) and the Carlsberg Foundation. The NMR laboratory at Aalborg University is supported by the Obel family foundation, the SparNord foundation, and the Carlsberg foundation. NMP and CVH thank Snedkermester Sophus Jacobsen og hustru Astrid Jacobsens Fond and Knud Højgaards Fond for a travel grant.

Supplementary materials

Supplementary material associated with this article can be found, in the online version, at doi:10.1016/j.ceca.2023.102831.

References

[1] H. Tidow, P. Nissen, Structural diversity of calmodulin binding to its target sites, FEBS J. 280 (2013) 5551–5565, https://doi.org/10.1111/FEBS.12296.
[2] K.L. Yap, J. Kim, K. Truong, M. Sherman, T. Yuan, M. Ikura, Calmodulin target database, J. Struct. Funct. Genomics. 1 (2000) 8–14, https://doi.org/10.1023/a:1011320027914.
[3] M. Nyegaard, M.T. Overgaard, M.T. Søndergaard, M. Vranas, E.R. Behr, L. L. Hildebrandt, J. Lund, P.L. Hedley, A.J. Camm, G. Wettrell, I. Fosdal, M. Christiansen, A.D. Børglum, Mutations in calmodulin cause ventricular tachycardia and sudden cardiac death, Am. J. Hum. Genet. 91 (2012) 703–712, https://doi.org/10.1016/j.ajhg.2012.08.015.
[4] A.B. Sorensen, M.T. Søndergaard, M.T. Overgaard, Calmodulin in a heartbeat, FEBS J. 280 (2013) 5511–5532, https://doi.org/10.1111/febs.12337.
[5] H.H. Jensen, M. Brohus, M. Nyegaard, M.T. Overgaard, Human Calmodulin Mutations, Front. Mol. Neurosci. 11 (2018) 396, https://doi.org/10.3389/fnmol.2018.00396.
[6] J.W. Hussey, W.B. Limpitikul, I.E. Dick, Calmodulin mutations in human disease, Channels 17 (2023), 2165278, https://doi.org/10.1080/19336950.2023.2165278.
[7] L. Crotti, C. Spazzolini, D.J. Tester, A. Ghidoni, A.-E. Baruteau, B.-M. Beckmann, E. R. Behr, J.S. Bennett, C.R. Bezzina, Z.A. Bhuiyan, A. Celiker, M. Cerrone, F. Dagradi, G.M. De Ferrari, S.P. Etheridge, M. Fatah, P. Garcia-Pavia, S. Al-Ghamdi, R.M. Hamilton, Z.N. Al-Hassnan, M. Horie, J. Jimenez-Jaimez, R. J. Kanter, J.P. Kaski, M.-C. Kotta, N. Lahrouchi, N. Makita, G. Norrish, H. H. Odland, S. Ohno, J. Papagiannis, G. Parati, N. Sekarski, K. Tveten, M. Vatta, G. Webster, A.A.M. Wilde, J. Wojciak, A.L. George, M.J. Ackerman, P.J. Schwartz, Calmodulin mutations and life-threatening cardiac arrhythmias: insights from the

International Calmodulinopathy Registry, Eur. Heart J. (2019) 2964–2975, https://doi.org/10.1093/eurheartj/ehz311.
[8] M. Nyegaard, M.T. Overgaard, The international calmodulinopathy registry: recording the diverse phenotypic spectrum of un-CALM hearts, Eur. Heart J. 40 (2019) 2976–2978, https://doi.org/10.1093/EURHEARTJ/EHZ463.
[9] L. Crotti, C. Spazzolini, M. Nyegaard, M.T. Overgaard, M.-C. Kotta, F. Dagradi, L. Sala, T. Aiba, M.D. Ayers, A. Baban, J. Barc, C.M. Beach, E.R. Behr, J.M. Bos, M. Cerrone, P. Covi, B. Cuneo, I. Denjoy, B. Donner, A. Elbert, H. Eliasson, S. P. Etheridge, M. Fukuyama, F. Girolami, R. Hamilton, M. Horie, M. Iascone, J. J. Jaimez, H.K. Jensen, P.J. Kannankeril, J.P. Kaski, N. Makita, C. Muñoz-Esparza, H.H. Odland, S. Ohno, J. Papagiannis, A.P. Porretta, C. Prandstetter, V. Probst, T. Robyns, E. Rosenthal, F. Rosés-Noguer, N. Sekarski, A. Singh, G. Spentzou, F. Stute, J. Tfelt-Hansen, J. Till, K.E. Tobert, J.M. Vinocur, G. Webster, A.A. M. Wilde, C.M. Wolf, M.J. Ackerman, P.J. Schwartz, Clinical presentation of calmodulin mutations: the International Calmodulinopathy Registry, Eur. Heart J. (2023), https://doi.org/10.1093/eurheartj/ehad418.
[10] N. Phillips, Trials of the heart, Nature 611 (2022) 218–223.
[11] M. Brohus, T. Arsov, D.A. Wallace, H.H. Jensen, M. Nyegaard, L. Crotti, M. Adamski, Y. Zhang, M.A. Field, V. Athanasopoulos, I. Baró, B.B. Ribeiro de Oliveira-Mendes, R. Redon, F. Charpentier, H. Raju, D. DiSilvestre, J. Wei, R. Wang, H. Rafehi, A. Kaspi, M. Bahlo, I.E. Dick, S.R.W. Chen, M.C. Cook, C. G. Vinuesa, M.T. Overgaard, P.J. Schwartz, Infanticide vs. inherited cardiac arrhythmias, EP Eur. 23 (2021) 441–450, https://doi.org/10.1093/europace/euaa272.
[12] D. Lewis, Science was heard': woman who was convicted of killing her children pardoned after inquiry, Nature 618 (2023) 445–446, https://doi.org/10.1038/d41586-023-01871-8.
[13] M. Brohus, A.-O. Busuioc, R. Wimmer, M. Nyegaard, M.T. Overgaard, Calmodulin mutations affecting Gly114 impair binding to the NaV1.5 IQ-domain, Front. Pharmacol. (2023) in press.
[14] K. Wang, C. Holt, J. Lu, M. Brohus, K.T. Larsen, M.T. Overgaard, R. Wimmer, F. Van Petegem, Arrhythmia mutations in calmodulin cause conformational changes that affect interactions with the cardiac voltage-gated calcium channel, Proc. Natl. Acad. Sci. U. S. A. 115 (2018) E10556–E10565, https://doi.org/10.1073/pnas.1808733115.
[15] C. Holt, L. Hamborg, K. Lau, M. Brohus, A.B. Sørensen, K.T. Larsen, C. Sommer, F. Van Petegem, M.T. Overgaard, R. Wimmer, The arrhythmogenic N53I variant subtly changes the structure and dynamics in the calmodulin N-domain, altering its interaction with the cardiac ryanodine receptor, J. Biol. Chem. 295 (2020) 7620–7634, https://doi.org/10.1074/jbc.RA120.013430.
[16] H. Kuboniwa, N. Tjandra, S. Grzesiek, H. Ren, C.B. Klee, A. Bax, Solution structure of calcium-free calmodulin, Nat. Struct. Biol. 2 (1995) 768–776, https://doi.org/10.1038/nsb0995-768.
[17] L.E. Kay, D.A. Torchia, A. Bax, Backbone dynamics of proteins as studied by 15 N inverse detected heteronuclear NMR spectroscopy: application to staphylococcal nuclease, Biochemistry 28 (1989) 8972–8979. http://www.ncbi.nlm.nih.gov/pubmed/2690953. accessed November 20, 2012.
[18] M. Kainosho, T. Torizawa, Y. Iwashita, T. Terauchi, A.Mei Ono, P. Güntert, Optimal isotope labelling for NMR protein structure determinations, Nature 440 (2006) 52–57, https://doi.org/10.1038/nature04525.
[19] M.T. Søndergaard, A.B. Sorensen, L.L. Skov, K. Kjaer-Sorensen, M.C. Bauer, M. Nyegaard, S. Linse, C. Oxvig, M.T. Overgaard, Calmodulin mutations causing catecholaminergic polymorphic ventricular tachycardia confer opposing functional and biophysical molecular changes, FEBS J. 282 (2015) 803–816, https://doi.org/10.1111/febs.13184.
[20] D. Bang, A.V. Gribenko, V. Tereshko, A.A. Kossiakoff, S.B. Kent, G.I. Makhatadze, Dissecting the energetics of protein α-helix C-cap termination through chemical protein synthesis, Nat. Chem. Biol. 2 (2006) 139–143, https://doi.org/10.1038/nchembio766.
[21] L. Serrano, J. Sancho, M. Hirshberg, A.R. Fersht, α-Helix stability in proteins: I. Empirical correlations concerning substitution of side-chains at the N and C-caps and the replacement of alanine by glycine or serine at solvent-exposed surfaces, J. Mol. Biol. 227 (1992) 544–559, https://doi.org/10.1016/0022-2836(92)90906-Z.
[22] R. Aurora, R. Srinivasan, G.D. Rose, Rules for α-helix termination by glycine, Science 264 (80) (1994) 1126–1130, https://doi.org/10.1126/SCIENCE.8178170.
[23] J.S. Richardson, D.C. Richardson, Amino acid preferences for specific locations at the ends of α helices, Science 240 (80) (1988) 1648–1652, https://doi.org/10.1126/SCIENCE.3381086.
[24] T.A. Craig, D.M. Watterson, F.G. Prendergast, J. Haiech, D.M. Roberts, Site-specific mutagenesis of the alpha-helices of calmodulin. Effects of altering a charge cluster in the helix that links the two halves of calmodulin - PubMed, J. Biol. Chem. 262 (1987) 3278–3284. https://pubmed.ncbi.nlm.nih.gov/3029108/. accessed March 17, 2023.
[25] J. Yang, M. Gao, J. Xiong, Z. Su, Y. Huang, Features of molecular recognition of intrinsically disordered proteins via coupled folding and binding, Protein Sci. 28 (2019) 1952–1965, https://doi.org/10.1002/pro.3718.
[26] D.-H. Kim, K.-H. Han, Target-binding behavior of IDPs via pre-structured motifs, Prog. Mol. Biol. Transl. Sci. 183 (2021) 187–247, https://doi.org/10.1016/bs.pmbts.2021.07.031.
[27] P.E. Wright, H.J. Dyson, Linking folding and binding, Curr. Opin. Struct. Biol. 19 (2009) 31–38, https://doi.org/10.1016/j.sbi.2008.12.003.
[28] O. Prakash, M. Held, L.F. McCormick, N. Gupta, L.Y. Lian, S. Antonyuk, L. P. Haynes, N.L. Thomas, N. Helassa, CPVT-associated calmodulin variants N53I and A102V dysregulate Ca2+ signalling via different mechanisms, J. Cell Sci. 135 (2022), https://doi.org/10.1242/JCS.258796.
[29] M. Muona, A.S. Aranko, V. Raulinaitis, H. Iwaï, Segmental isotopic labeling of multi-domain and fusion proteins by protein trans-splicing in vivo and in vitro, Nat. Protoc. 5 (2010) 574–587, https://doi.org/10.1038/NPROT.2009.240.
[30] M. Bhagawati, T.M.E. Terhorst, F. Füsser, S. Hoffmann, T. Pasch, S. Pietrokovski, H.D. Mootz, A mesophilic cysteine-less split intein for protein trans-splicing applications under oxidizing conditions, Proc. Natl. Acad. Sci. U. S. A. 116 (2019) 22164–22172, https://doi.org/10.1073/PNAS.1909825116/-/DCSUPPLEMENTAL.
[31] N.A. Farrow, R. Muhandiram, A.U. Singer, S.M. Pascal, C.M. Kay, G. Gish, S. E. Shoelson, T. Pawson, J.D. Forman-Kay, L.E. Kay, Backbone dynamics of a free and phosphopeptide-complexed Src homology 2 domain studied by 15 N NMR relaxation, Biochemistry 33 (1994) 5984–6003. http://www.ncbi.nlm.nih.gov/pubmed/7514039. accessed November 7, 2012.
[32] M. Tollinger, N.R. Skrynnikov, F.A. Mulder, J.D. Forman-Kay, L.E. Kay, Slow dynamics in folded and unfolded states of an SH3 domain, J. Am. Chem. Soc. 123 (2001) 11341–11352, https://doi.org/10.1021/ja011300z.
[33] J.E. Masse, R. Keller, AutoLink: automated sequential resonance assignment of biopolymers from NMR data by relative-hypothesis-prioritization-based simulated logic, J. Magn. Reson. 174 (2005) 133–151.
[34] R. Keller, The Computer Aided Resonance Assignment Tutorial, 1, CANTINA Verlag, Goldau (Switzerland), 2004.
[35] P. Klukowski, R. Riek, P. Güntert, Rapid protein assignments and structures from raw NMR spectra with the deep learning technique ARTINA, Nat. Commun. 13 (2022) 6151, https://doi.org/10.1038/S41467-022-33879-5.
[36] E. Schmidt, P. Güntert, A new algorithm for reliable and general NMR resonance assignment, J. Am. Chem. Soc. 134 (2012) 12817–12829, https://doi.org/10.1021/ja305091n.
[37] P. Güntert, L. Buchner, Combined automated NOE assignment and structure calculation with CYANA, J. Biomol. NMR. 62 (2015) 453–471.
[38] P. Güntert, Calculating protein structures from NMR data, Methods Mol. Biol. 60 (1997) 157–194, 10.1385/0-89603-309-0:157.
[39] P. Güntert, C. Mumenthaler, K. Wüthrich, Torsion angle dynamics for NMR structure calculation with the new program DYANA, J. Mol. Biol. 273 (1997) 283–298.
[40] T. Herrmann, P. Güntert, K. Wüthrich, Protein NMR structure determination with automated NOE-identification in the NOESY spectra using the new software ATNOS, J. Biomol. NMR 24 (2002) 171–189.
[41] Y. Shen, A. Bax, Protein backbone and sidechain torsion angles predicted from NMR chemical shifts using artificial neural networks, J. Biomol. NMR 56 (2013) 227–241, https://doi.org/10.1007/s10858-013-9741-y.
[42] E. Krieger, G. Vriend, YASARA View - molecular graphics for all devices - from smartphones to workstations, Bioinformatics 30 (2014) 2981–2982, https://doi.org/10.1093/bioinformatics/btu426.
[43] E. Krieger, G. Koraimann, G. Vriend, Increasing the precision of comparative models with YASARA NOVA–a self-parameterizing force field, Proteins 47 (2002) 393–402.
[44] E. Krieger, K. Joo, J. Lee, J. Lee, S. Raman, J. Thompson, M. Tyka, D. Baker, K. Karplus, Improving physical realism, stereochemistry and side-chain accuracy in homology modeling: four approaches that performed well in CASP8, Proteins 77 (2009) 114–122, https://doi.org/10.1002/prot.22570.
[45] N.J. Greenfield, Using circular dichroism collected as a function of temperature to determine the thermodynamics of protein unfolding and binding interactions, Nat. Protoc. 16 (1) (2006) 2527–2535, https://doi.org/10.1038/NPROT.2006.204, 2006.
[46] L. Masino, S.R. Martin, P.M. Bayley, Ligand binding and thermodynamic stability of a multidomain protein, calmodulin, Protein Sci. 9 (2000) 1519–1529, https://doi.org/10.1110/ps.9.8.1519.